

# Hybrid STAR-RIS Enabled Integrated Sensing and Communication

Zehra Yigit, *Member, IEEE*, Ertugrul Basar, *Fellow, IEEE*

**Abstract**—Integrated sensing and communication (ISAC) is recognized as one of the key enabling technologies for sixth-generation (6G) wireless communication networks, facilitating diverse emerging applications and services in an energy and cost-efficient manner. This paper proposes a multi-user multi-target ISAC system to enable full-space coverage for communication and sensing tasks. The proposed system employs a hybrid simultaneous transmission and reflection reconfigurable intelligent surface (STAR-RIS) comprising active transmissive and passive reflective elements. In the proposed scheme, the passive reflective elements support communication and sensing links for nearby communication users and sensing targets, while low-power active transmissive elements are deployed to improve sensing performance and overcome high path attenuation due to multi-hop transmission for remote targets. Moreover, to optimize the transmissive/reflective coefficients of the hybrid STAR-RIS, a semi-definite relaxation (SDR)-based algorithm is proposed. Furthermore, to evaluate sensing performance, signal-to-interference-noise ratio (SINR) and Cramer-Rao bound (CRB) metrics have been derived and investigated via conducting extensive computer simulations.

**Index Terms**—Integrated sensing and communication (ISAC), simultaneous transmission and reflection reconfigurable intelligent surface (STAR-RIS), multi-user, multi-target, active RIS.

## I. INTRODUCTION

Sixth-generation (6G) networks are envisioned to provide intelligent, secure, and ubiquitous wireless connectivity via enhanced and new usage scenarios with advanced capabilities [1]. In this vision, integrated sensing and communication (ISAC) stands out as a key enabling technology that offers a unified platform for hardware resources, spectrum, and signal processing framework to enable simultaneous communication and sensing functionalities [1, 2]. This integration brings mutual benefits of communication and sensing via enhancing the hardware, spectrum, energy, and cost efficiencies while defining new sensing-related environmental-aware applications and services, including vehicle-to-everything (V2X), remote sensing, smart cities, smart healthcare, and environmental monitoring [3].

Although ISAC has gained significant attention in the literature over the past few years, it has a longstanding history

of research under various names, such as joint radar and communication (JRC) [4], joint communication and radar (JCR) [5] and dual function radar communication (DFRC) [6]. The primary difference between JRC and JCR lies in their respective emphasis: JRC prioritizes radar-centric designs with integrated communication capabilities, while JCR emphasizes communication-centric designs enhanced with radar functionalities. On the other hand, DFRC refers to a unified platform that utilizes shared waveforms for both communication and sensing tasks [5].

Reconfigurable intelligent surface (RIS)-empowered communication is another emerging technology that offers energy and cost-efficient solutions for ubiquitous connectivity in next generation networks [7, 8]. RISs are planar metasurfaces consisting a large number of passive reflective elements to efficiently modify wireless propagation environment, thereby paving the way of achieving the vision for a smart radio environment [9, 10]. By dynamically shaping and managing the propagation of electromagnetic waves, RISs are primarily utilized to improve signal quality [11, 12], enhance channel capacity [13], mitigate inter-user interference [14] and ensure physical layer security [15]. However, recent studies indicate a growing interest in deploying RIS for sensing applications [16–18] that mostly focus on sensing performance [19] and beamforming optimization [20, 21] of RIS-assisted single-target ISAC systems.

Although traditional reflection-only passive RISs can improve communication and sensing performance of ISAC systems in challenging non line-of-sight (NLOS) conditions [17, 18], they struggle to mitigate multiplicative path attenuation due to multi-hop transmission of the sensing link. This limitation restricts their deployment to locations near the transmitter and/or receiver to achieve noticeable performance gains [22]. To overcome this limitation and enhance performance of sensing link, active RIS-assisted ISAC systems, which incorporates additional power amplifiers to modify not only the phase but also the magnitude of an incident electromagnetic wave, has been proposed [23, 24].

More recently, simultaneous transmission and reflection RIS (STAR-RIS)-assisted ISAC systems have been introduced to achieve full-space coverage and enable flexible deployment of base-stations (BSs), sensing targets, and communication users, independent of their positioning relative to the RIS [25–27]. In [25], a single-target, multi-user ISAC system is proposed, utilizing a STAR-RIS equipping a portion of the surface with one-side sensing-capable elements dedicated to serving sensing targets, while passive transmissive elements are employed to cater to communication users. A multi-target

Z. Yigit is with Turkcell Iletisim Hizmetleri Inc., 6GEN Lab., E-mail: zehra.yigit@turkcell.com.tr.

E. Basar is with the Communications Research and Innovation Laboratory (CoreLab), Department of Electrical and Electronics Engineering, Koç University, Sariyer 34450, Istanbul, Turkey. E-mail: ebasar@ku.edu.tr.

This work was supported by The Scientific and Technological Research Council of Turkey (TUBITAK) through the 1515 Frontier Research and Development Laboratories Support Program under Project 5229901 - 6GEN. Lab: 6G and Artificial Intelligence Laboratory, and also Grant 120E401.

multi-user ISAC scenario deploying a STAR-RIS with bi-directional sensing elements is presented in [26]. In addition, in [27], receive antennas are positioned on both sides of the STAR-RIS to mitigate severe path attenuation, enabling multi-target multi-user ISAC transmissions on both sides of the STAR-RIS.

Motivated by the aforementioned studies, to further improve energy efficiency of RIS-assisted ISAC systems while achieving full-space coverage, this paper proposes a novel multi-target multi-user ISAC transmission system, utilizing a dual-sided STAR-RIS, with each side offering both reflective and transmissive capabilities. In the proposed scheme, to address severe signal power degradation due to multi-hop transmission, a hybrid STAR-RIS with active transmissive and passive reflective elements is utilized. Unlike [25, 26] that employ sensing capable elements and additional receive antennas [27], leading hardware and implementation complexity, the proposed scheme enables an efficient multi-target and multi-user transmission on both sides of STAR-RIS with a more cost-effective and power efficient manner. Moreover, to optimize the transmissive/reflective coefficients of the hybrid STAR-RIS, a non-convex optimization problem is formulated, which is solved via a semi-definite relaxation (SDR)-based approach implemented through CVX toolbox [28]. Furthermore, comprehensive simulations are conducted to evaluate target signal-to-interference-noise ratio (SINR) and Cramer-Rao bound (CRB) to estimate two-dimensional (2D) angles of departure (AoDs) of the sensing targets.

The rest of the paper is organized as follows. In Section II, the proposed system model is introduced. Section III provides derivations for sensing performance metrics including target SINR and CRB for 2D AoDs estimation, followed by the proposed optimization algorithm. In Section IV, the numerical results are presented, and this paper concludes with Section V.

*Notation:* Throughout this paper, vectors and matrices are denoted by bold-face lower letter and bold-face upper letter, respectively.  $\mathbb{C}^{K \times L}$  represents the space of a complex matrix with dimensions  $K \times L$ .  $|x|$  stands for absolute value of scalar  $x$ , while  $\|\mathbf{X}\|$  is the Frobenius norm of matrix  $\mathbf{X}$ .  $\mathbf{X}^{-1}$ ,  $\mathbf{X}^T$  and  $\mathbf{X}^H$  represent inverse, transposition and Hermitian of the matrix  $\mathbf{X}$ , respectively. For  $\mathbf{x}$  being a vector,  $\text{diag}(\mathbf{x})$  stands for a diagonal matrix whose diagonal elements are equal to elements of the vector  $\mathbf{x}$ .  $\text{vec}(\mathbf{X})$  is vectorizing operation,  $\text{rect}(\cdot)$  is rectangular function and  $\text{Tr}(\mathbf{X})$  is trace value.  $\mathbf{I}$  denotes identity matrix, while  $\mathbf{1}$  stands for a vector with all-ones elements.  $\Re\{\cdot\}$  and  $\Im\{\cdot\}$  represents real and imaginary components of a complex number, respectively.  $\mathcal{CN}(\mu, \sigma^2)$  denotes distribution of a complex Gaussian random variable with mean  $\mu$  and variance  $\sigma^2$ .

## II. SYSTEM MODEL

In this section, following an introduction to active and passive RISs and the STAR-RIS model, system model for the proposed hybrid STAR-RIS-enabled ISAC is presented.

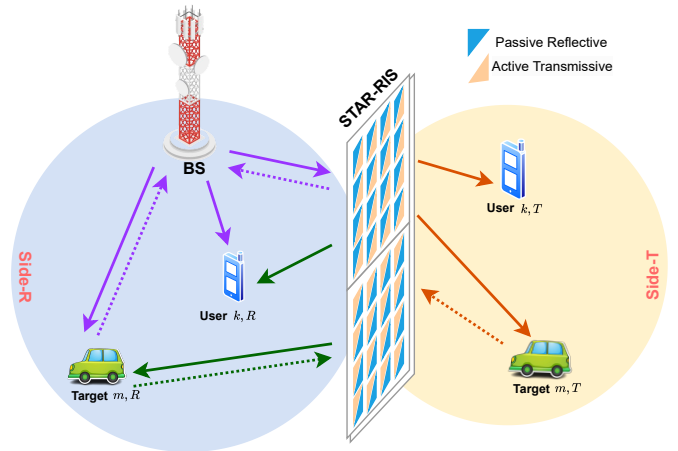


Fig. 1. System model of hybrid RIS-assisted ISAC.

### A. Active vs. Passive RIS

Multiplicative path attenuation poses a significant challenge in RIS-assisted communication systems [29]. Passive RIS, equipped with reflective elements that can solely manipulate the phases of the incident signals, struggles to overcome this hurdle [30]. To address this challenge, the concept of active RIS, capable of simultaneously controlling the magnitudes and phases of incident signals, has been proposed [22, 30–32]. This approach involves integrating active RIS elements with low-power reflective-type amplifiers, such as tunneling reflection amplifiers [33] and amplifying reflect arrays [34]. While this integration allows for the adjustment of the magnitudes of incident waves, it comes with the trade-off of an increase in power consumption and the unavoidable introduction of thermal noise. Additionally, the reflection coefficient of an active RIS element,  $\Omega_a$ , and a passive RIS element,  $\Omega_p$ , can be defined as

$$\Omega_a = \xi_a e^{j\phi_a} \text{ for } \xi_a > 1, \text{ and } \phi_a \in [-\pi, \pi] \quad (1)$$

$$\Omega_p = \xi_p e^{j\phi_p} \text{ for } \xi_p \leq 1, \text{ and } \phi_p \in [-\pi, \pi] \quad (2)$$

where  $|\xi_i|$  and  $\phi_i$  respectively are the magnitude and phase of the corresponding RIS element for  $i \in \{a, p\}$ .

### B. STAR-RIS Model

Unlike conventional RIS systems, which offer half-space ( $180^\circ$ ) coverage and constrain the transmitter and receiver(s) to be located on the same side of the RIS [14], the STAR-RIS concept has been proposed to extend the RIS coverage [35]. This is achieved by enabling simultaneous reflection and transmission of the incident signal, offering further flexibility in the deployment of transmitter and receiver(s) [35]. In STAR-RIS, each of the STAR-RIS element splits the incoming signal from BS in two parts: one part of the signal is reflected on the same side of the incident signal (reflection side), while the second part is transmitted to the opposite side of the incident signal (transmission side) [35]. Therefore, the transmission and reflection coefficients of the STAR-RIS can be modeled as  $\Omega_t = \xi_t e^{j\phi_t}$  and  $\Omega_r = \xi_r e^{j\phi_r}$ , respectively. It is worth noting

that a STAR-RIS can have independent transmission/reflection magnitude gains, while its phase shifts can be modeled either as coupled or independent [36].

### C. Hybrid STAR-RIS-Enabled ISAC

The system model of the proposed hybrid STAR-RIS-assisted ISAC is illustrated in Fig. 1. In the proposed system, a uniform linear array (ULA) BS with  $T_x$  antennas communicates with  $K$  single-antenna users, while simultaneously performing  $M$  point targets detection. It is assumed that the coverage space of the BS is split into two parts: transmission (Side- $T$ ) and reflection (Side- $R$ ) by a hybrid STAR-RIS with a uniform planar array (UPA) consisting  $N$  transmissive/reflective elements. To enable two-side target detection and alleviate path attenuation, the hybrid STAR-RIS operates as a dual-sided STAR-RIS, with ‘‘STAR’’ functionality present on both sides [36, 37], incorporating passive reflective and active transmissive elements. Alternatively, it can be constructed using two adjacent conventional STAR-RIS units oriented oppositely, each featuring active transmissive and passive reflective elements. However, in this paper, for the simplicity of presentation, a dual-sided STAR-RIS with unit-gain passive reflective ( $\xi_{r,n} = 1$ ) and active transmissive elements ( $\xi_{t,n} > 1$ ) is considered, where  $n \in \{1, 2, \dots, N\}$ . Please note that, in the proposed scheme, transmissive and reflective components of the dual-sided hybrid STAR-RIS are assumed to be identical in two directions (from Side- $T$  to Side- $R$ , from Side- $R$  to Side- $T$ ), while their phase-shifts and magnitudes are independently configured [36]. Consequently, the transmission and reflection coefficients of the hybrid STAR-RIS with  $N$  elements in both directions can be defined as

$$\Phi_t \in \mathbb{C}^{N \times N} = \text{diag} \left( \xi_{t,1} e^{j\phi_{t,1}}, \xi_{t,2} e^{j\phi_{t,2}}, \dots, \xi_{t,N} e^{j\phi_{t,N}} \right) \quad (3)$$

$$\Phi_r \in \mathbb{C}^{N \times N} = \text{diag} \left( e^{j\phi_{r,1}}, e^{j\phi_{r,2}}, \dots, e^{j\phi_{r,N}} \right) \quad (4)$$

where  $\Phi_t$  and  $\Phi_r$  are the transmission and reflection matrices, respectively.

In this study, it is assumed that  $K_R$  users and  $M_R$  targets at Side- $R$  receive both direct signals from the BS and indirect signals reflected by the hybrid STAR-RIS, while  $K_T$  users and  $M_T$  targets at Side- $T$  can only perceive transmitted signals through the hybrid STAR-RIS, where  $K = K_R + K_T$  and  $M = M_R + M_T$ . It is important to note that throughout the paper, regardless of their distances from the BS, the communication users and sensing targets on Side- $R$  who are located within the same region as the base station (BS) are classified as ‘‘nearby’’, whereas those on Side- $T$  are referred as ‘‘remote’’.

In the proposed scheme, to enable simultaneous communication and sensing, the BS transmits following joint signal at  $l$ th time instance, represented by  $\mathbf{x}(l) \in \mathbb{C}^{T_x \times 1}$  becomes

$$\mathbf{x}(l) = \sum_{p=1}^K \mathbf{w}_{c,p} c_p(l) + \sum_{q=1}^M \mathbf{w}_{s,q} s_q(l) \quad (5)$$

$$= \mathbf{W} \tilde{\mathbf{x}}(l) \quad (6)$$

where  $\mathbf{W} \in \mathbb{C}^{T_x \times (K+M)}$  is the overall beamforming matrix. Here,  $c_p(l)$  and  $s_q(l)$  are transmit signals for  $p$ th communication user and  $q$ th sensing target, while  $\mathbf{w}_{c,p} \in \mathbb{C}^{T_x \times 1}$  and  $\mathbf{w}_{s,q} \in \mathbb{C}^{T_x \times 1}$  are their corresponding beamforming vectors, respectively. Therefore, the covariance matrix of the transmit signal can be defined as

$$\mathbf{R}_x = \mathbb{E} \left\{ \mathbf{x}(l) \mathbf{x}^H(l) \right\} \quad (7)$$

and transmit power at the BS is calculated as

$$\begin{aligned} P_{\text{BS}} &\geq \sum_{p=1}^K \mathbf{w}_{c,p}^H \mathbf{w}_{c,p} + \sum_{q=1}^M \mathbf{w}_{s,q}^H \mathbf{w}_{s,q} \\ &\geq \text{Tr}(\mathbf{R}_x). \end{aligned} \quad (8)$$

In the proposed scheme, communication signals are generated as complex Gaussian random variables with zero mean and unit variance, i.e.,  $\mathbb{E} \left\{ \mathbf{c}(l) \mathbf{c}^H(l) \right\} = \mathbf{I}_K$ , while sensing signals are generated as frequency modulated continuous wave (FMCW) signals [38] as follows

$$s_q(l) = \sum_{\tau=1}^{L_c} A_\tau \text{rect} \left( \frac{l - (\tau - \frac{1}{2} T_c)}{T_c} \right) \cos \left( 2\pi f_c l + \pi \frac{B_w}{L} l^2 \right) \quad (9)$$

where  $L_c$  is the number of chips,  $L$  is the chirp length,  $T_c = L/L_c$  is the chip duration, the  $A_\tau$  is the amplitude of the signal at the  $\tau$ -th time block,  $A_\tau \in \{-1, 1\}$ ,  $f_c$  is the carrier frequency and  $B_w$  is the bandwidth. Thus,  $\mathbb{E} \left\{ \mathbf{c}(l) \mathbf{s}^H(l) \right\} = \mathbf{0}_{K \times M}$ .

### D. Communication Model

In the proposed system, all communication channels are modeled by Rician fading channels, and the channels between BS-STAR-RIS (BS-RIS), BS-User  $k$  at Side- $R$  (BS- $U_{k,R}$ ) and STAR-RIS-User  $k$  at Side  $i$  (RIS- $U_{k,i}$ ) are respectively represented by  $\mathbf{G} \in \mathbb{C}^{N \times T_x}$ ,  $\mathbf{g}_{k,R} \in \mathbb{C}^{1 \times T_x}$  and  $\mathbf{h}_{k,i} \in \mathbb{C}^{1 \times N}$ , where  $i \in \mathcal{S} = \{T, R\}$  and  $k \in \{1, \dots, K_i\}$ . Therefore, communication channels  $\mathbf{D}_c \in \{\mathbf{G}, \mathbf{g}_{k,R}, \mathbf{h}_{k,i}\}$  are given as:

$$\mathbf{D}_c = \sqrt{\alpha_c} \left( \sqrt{\frac{\kappa}{1+\kappa}} \mathbf{D}_c^{\text{LOS}} + \sqrt{\frac{1}{1+\kappa}} \mathbf{D}_c^{\text{NLOS}} \right) \quad (10)$$

where  $\mathbf{D}_c^{\text{LOS}}$  represents the LOS component,  $\mathbf{D}_c^{\text{NLOS}}$  stands for the NLOS component,  $\kappa$  is the Rician factor and  $\alpha_c = \alpha_0 d_c^{-\rho} \in \{\alpha_{\text{BS-RIS}}, \alpha_{\text{BS-}U_{k,R}}, \alpha_{\text{RIS-}U_{k,i}}\}$  denotes corresponding path attenuation, for  $\alpha_0$  being the reference path loss at 1 meter (m),  $\rho$  being path-loss exponent and  $d_c \in \{d_{\text{BS-RIS}}, d_{\text{BS-}U_{k,R}}, d_{\text{RIS-}U_{k,i}}\}$  being the corresponding distance. Here, each element of  $\mathbf{D}_c^{\text{NLOS}}$  component is assumed to be generated by independent and identically distributed (i.i.d.) complex Gaussian random variables following  $\mathcal{CN}(0, 1)$  distribution, while  $\mathbf{D}_c^{\text{LOS}}$  component is deterministic channel generated by steering vectors. Therefore, the overall  $\mathbf{D}_c$  channel follows  $\mathcal{CN}(\sqrt{\alpha_c} \sqrt{\frac{\kappa}{1+\kappa}} \mathbf{D}_c^{\text{LOS}}, \alpha_c \frac{1}{1+\kappa} \mathbf{I})$ .

Using steering vectors, the LOS component  $\mathbf{G}^{\text{LOS}} \in \mathbb{C}^{N \times T_x}$  of the channel between BS-STAR-RIS is generated as:

$$\mathbf{G}^{\text{LOS}} = \mathbf{b}^H(\varphi_{c,h}^{\text{RIS}}, \varphi_{c,v}^{\text{RIS}}) \mathbf{a}(\theta_{c,h}^{\text{RIS}}, \theta_{c,v}^{\text{RIS}}) \quad (11)$$

where  $\mathbf{a}(\theta_{c,h}^{\text{RIS}}, \theta_{c,v}^{\text{RIS}}) \in \mathbb{C}^{1 \times T_x}$  and  $\mathbf{b}(\varphi_{c,h}^{\text{RIS}}, \varphi_{c,v}^{\text{RIS}}) \in \mathbb{C}^{1 \times N}$  are the ULA and UPA array factors of BS and hybrid STAR-RIS, respectively. Here,  $N = N_x \times N_y$  with  $N_x$  and  $N_y$  representing the number of hybrid STAR-RIS elements located horizontally and vertically on  $x$ - $y$  plane, respectively.  $\theta_{c,h}^{\text{RIS}}, \theta_{c,v}^{\text{RIS}}$  are horizontal and vertical AoDs from BS towards RIS, while  $\varphi_{c,h}^{\text{RIS}}, \varphi_{c,v}^{\text{RIS}}$  are the horizontal, vertical angles of arrival (AoA) at RIS, respectively. Here,  $\mathbf{a}(\theta_{c,h}^{\text{RIS}}, \theta_{c,v}^{\text{RIS}})$  and  $\mathbf{b}(\varphi_{c,h}^{\text{RIS}}, \varphi_{c,v}^{\text{RIS}})$  array factors are given as

$$\mathbf{a}(\theta_{c,h}^{\text{RIS}}, \theta_{c,v}^{\text{RIS}}) = [1, \dots, e^{j\eta_{\text{BS}}(T_x-1) \sin(\theta_{c,h}^{\text{RIS}}) \cos(\theta_{c,v}^{\text{RIS}})}] \quad (12)$$

$$\mathbf{b}(\varphi_{c,h}^{\text{RIS}}, \varphi_{c,v}^{\text{RIS}}) = \mathbf{b}^x(\varphi_{c,h}^{\text{RIS}}, \varphi_{c,v}^{\text{RIS}}) \otimes \mathbf{b}^y(\varphi_{c,h}^{\text{RIS}}, \varphi_{c,v}^{\text{RIS}}) \quad (13)$$

where  $\eta_{\text{BS}} = \frac{2\pi}{\lambda} d_{\text{BS}}$  for  $\lambda$  wavelength and  $d_{\text{BS}}$  distance between two adjacent transmit/receive antennas at BS, respectively. Here,  $\mathbf{b}^x(\varphi_{c,h}^{\text{RIS}}, \varphi_{c,v}^{\text{RIS}}) \in \mathbb{C}^{1 \times N_x}$  and  $\mathbf{b}^y(\varphi_{c,h}^{\text{RIS}}, \varphi_{c,v}^{\text{RIS}}) \in \mathbb{C}^{1 \times N_y}$  are respectively steering vectors of STAR-RIS in  $x$  and  $y$  dimensions given as

$$\mathbf{b}^x(\varphi_{c,h}^{\text{RIS}}, \varphi_{c,v}^{\text{RIS}}) = [1, \dots, e^{j\eta_{\text{RIS}}(N_x-1) \sin(\varphi_{c,h}^{\text{RIS}}) \cos(\varphi_{c,v}^{\text{RIS}})}] \quad (14)$$

$$\mathbf{b}^y(\varphi_{c,h}^{\text{RIS}}, \varphi_{c,v}^{\text{RIS}}) = [1, \dots, e^{j\eta_{\text{RIS}}(N_y-1) \sin(\varphi_{c,h}^{\text{RIS}}) \sin(\varphi_{c,v}^{\text{RIS}})}] \quad (15)$$

where  $\eta_{\text{RIS}} = \frac{2\pi}{\lambda} d_{\text{RIS}}$  for  $d_{\text{RIS}}$  being horizontal and vertical distance between two adjacent elements at STAR-RIS. Therefore, (13) can be simply rewritten as

$$\mathbf{b}(\varphi_{c,h}^{\text{RIS}}, \varphi_{c,v}^{\text{RIS}}) = e^{j\eta_{\text{RIS}} \mathbf{k}(\varphi_{c,h}^{\text{RIS}}, \varphi_{c,v}^{\text{RIS}})} \quad (16)$$

where  $\mathbf{k}(\varphi_{c,h}^{\text{RIS}}, \varphi_{c,v}^{\text{RIS}}) \in \mathbb{C}^{1 \times N} = \mathbf{k}_x \sin(\varphi_{c,h}^{\text{RIS}}) \cos(\varphi_{c,v}^{\text{RIS}}) + \mathbf{k}_y \sin(\varphi_{c,h}^{\text{RIS}}) \sin(\varphi_{c,v}^{\text{RIS}})$ . Here,  $\mathbf{k}_x \in \mathbb{C}^{1 \times N} = \mathbf{e}_x \otimes \mathbf{1}_{N_y}$  and  $\mathbf{k}_y \in \mathbb{C}^{1 \times N} = \mathbf{1}_{N_x} \otimes \mathbf{e}_y$  are with scalar components for  $\mathbf{e}_x \in \mathbb{C}^{1 \times N_x} = [0, 1 \dots, N_x-1]$  and  $\mathbf{e}_y \in \mathbb{C}^{1 \times N_y} = [0, 1 \dots, N_y-1]$ .

Similarly, the LOS channel components of the channel between BS- $U_{k,R}$  and RIS- $U_{k,i}$  can be generated as  $\mathbf{g}_{k,R}^{\text{LOS}} = \mathbf{a}(\theta_{c,h}^{k,R}, \theta_{c,v}^{k,R}) \in \mathbb{C}^{1 \times T_x}$  and  $\mathbf{h}_{k,i}^{\text{LOS}} = \mathbf{b}(\varphi_{c,h}^{k,i}, \varphi_{c,v}^{k,i}) \in \mathbb{C}^{1 \times N}$ , where  $\{\theta_{c,h}^{k,R}, \theta_{c,v}^{k,R}\}$  and  $\{\varphi_{c,h}^{k,i}, \varphi_{c,v}^{k,i}\}$  are horizontal and vertical AoD pairs from the BS towards  $U_{k,R}$  and from STAR-RIS towards  $U_{k,i}$  at Side  $i \in \mathcal{S} = \{T, R\}$ , respectively. Then, following ULA and UPA in (12) and (16)  $\mathbf{a}(\theta_{c,h}^{k,R}, \theta_{c,v}^{k,R})$  and  $\mathbf{b}(\varphi_{c,h}^{k,i}, \varphi_{c,v}^{k,i})$  can be given as

$$\mathbf{a}(\theta_{c,h}^{k,R}, \theta_{c,v}^{k,R}) = [1, \dots, e^{j\eta_{\text{BS}}(T_x-1) \sin(\theta_{c,h}^{k,R}) \cos(\theta_{c,v}^{k,R})}] \quad (17)$$

$$\mathbf{b}(\varphi_{c,h}^{k,i}, \varphi_{c,v}^{k,i}) = e^{j\eta_{\text{RIS}} \mathbf{k}(\varphi_{c,h}^{k,i}, \varphi_{c,v}^{k,i})} \quad (18)$$

where  $\mathbf{k}(\varphi_{c,h}^{k,i}, \varphi_{c,v}^{k,i}) \in \mathbb{C}^{1 \times N} = \mathbf{k}_x \sin(\varphi_{c,h}^{k,i}) \cos(\varphi_{c,v}^{k,i}) + \mathbf{k}_y \sin(\varphi_{c,h}^{k,i}) \sin(\varphi_{c,v}^{k,i})$ . Then, following (10), the received signal at  $U_{k,T}$  that perceives the transmit signals from the BS over the the active transmissive elements of the hybrid STAR-RIS becomes

$$y_c^{k,T}(l) = \mathbf{h}_{k,T} \Phi_t \mathbf{G} \mathbf{x}(l) + \mathbf{h}_{k,T} \Phi_t \mathbf{v}_1 + n_c^{k,T}(l) \quad (19)$$

where  $n_c^{k,T}(l) \in \mathcal{CN}(0, \sigma_{n_c}^2)$  is the static additive white Gaussian noise (AWGN) sample and  $\mathbf{v}_1 \in \mathbb{C}^{N \times 1}$  is the internal thermal noise generated from active STAR-RIS elements whose each element is i.i.d. and follows  $\mathcal{CN}(0, \sigma_{v_1}^2)$  distribution.

Likewise, for the communication users at Side- $R$  that receive signals from BS through the direct path and reflected

path over passive reflective elements of the hybrid STAR-RIS, the received signal at  $U_{k,R}$  can be given as

$$y_c^{k,R}(l) = (\mathbf{h}_{k,R} \Phi_r \mathbf{G} + \mathbf{g}_{k,R}) \mathbf{x}(l) + n_c^{k,R}(l) \quad (20)$$

where  $n_c^{k,R}(l) \sim \mathcal{CN}(0, \sigma_{n_c}^2)$  is the overall noise term.

### E. Sensing Model

In the proposed system, the paths from the BS and hybrid STAR-RIS towards the targets are deterministic channels and constructed using steering vectors. The channel between the STAR-RIS and the target  $m$  at Side- $i$  ( $O_{m,i}$ ) can be given in terms of the AoD pair of  $\{\varphi_h^{m,i}, \varphi_v^{m,i}\}$  as follows

$$\mathbf{b}(\varphi_{s,h}^{m,i}, \varphi_{s,v}^{m,i}) = e^{j\eta_{\text{RIS}} \mathbf{k}(\varphi_{s,h}^{m,i}, \varphi_{s,v}^{m,i})} \quad (21)$$

where  $\mathbf{b}(\varphi_{s,h}^{m,i}, \varphi_{s,v}^{m,i}) \in \mathbb{C}^{1 \times N}$ ,  $\mathbf{k}(\varphi_{s,h}^{m,i}, \varphi_{s,v}^{m,i}) \in \mathbb{C}^{1 \times N} = \mathbf{k}_x \sin(\varphi_{s,h}^{m,i}) \cos(\varphi_{s,v}^{m,i}) + \mathbf{k}_y \sin(\varphi_{s,h}^{m,i}) \sin(\varphi_{s,v}^{m,i})$ . Thus, the received echo signal at the BS from the  $m$ th sensing target on Side- $T$  ( $O_{m,T}$ ) follows the path of BS→STAR-RIS→ $O_{m,T}$ →STAR-RIS→BS. In order to mitigate severe path attenuation due to this multi-hop transmission, the considered dual-sided hybrid STAR-RIS utilizes active elements in transmission mode in both directions. Then, the received echo signal collected at the BS due to the sensing target  $O_{m,T}$  becomes

$$y_s^{m,T}(l) = \beta_{\text{RIS}}^{m,T} \mathbf{G}^H \Phi_t^H \mathbf{B}_m \Phi_t \mathbf{G} \mathbf{x}(l) + \tilde{\mathbf{n}}_s^{m,T}(l) \quad (22)$$

where  $m \in \{1, \dots, M_T\}$ ,  $\beta_{\text{RIS}}^{m,T}$  is the round-trip path attenuation,  $\mathbf{B}_m = \mathbf{b}^H(\varphi_{s,h}^{m,T}, \varphi_{s,v}^{m,T}) \mathbf{b}(\varphi_{s,h}^{m,T}, \varphi_{s,v}^{m,T})$ ,  $\tilde{\mathbf{n}}_s^{m,T}(l) = \mathbf{G}^H \Phi_t^H \mathbf{B}_m \Phi_t \mathbf{v}_1(l) + \mathbf{G}^H \Phi_t^H \mathbf{v}_2(l) + \mathbf{n}_s^{m,T}(l)$  is the overall noise samples vector including thermal noise of active transmissive elements and static noise in the channel for  $\mathbf{n}_s^{m,T}(l)$  being static noise and following  $\sim \mathcal{CN}(0, \sigma_{n_s}^2 \mathbf{I})$  distribution, while  $\mathbf{v}_1(l)$  and  $\mathbf{v}_2(l)$  are the thermal noise vectors with the  $\mathcal{CN}(0, \sigma_{v_1}^2 \mathbf{I})$  and  $\mathcal{CN}(0, \sigma_{v_2}^2 \mathbf{I})$  distributions, respectively. Here, for the sake of simplicity, the thermal and static noise variances are assumed to be  $\sigma_{n_s}^2 = \sigma_{v_1}^2 = \sigma_{v_2}^2$ . It is important to note that for  $P_A = \text{Tr}(\Phi_t^H \Phi_t) = \sum_{n=1}^{N-1} |\xi_{t,n}|^2$  being the overall amplification factor of the active transmissive elements, a low  $P_A$  amplification factor implies that the internal thermal noise of the active transmissive STAR-RIS elements remains negligible. This is because the path attenuation terms in the first and second expressions of  $\tilde{\mathbf{n}}_s^{m,T}(l)$  make them insignificant, resulting in  $\tilde{\mathbf{n}}_s^{m,T}(l) \approx \mathbf{n}_s^{m,T}(l)$ . In this case, the distribution of  $\tilde{\mathbf{n}}_s^{m,T}(l)$  approximates to  $\sim \mathcal{CN}(0, \sigma_{n_s}^2 \mathbf{I})$  where  $\sigma_{n_s}^2 = \sigma_{n_s}^2$ . On the other hand, for very high  $P_A$  values, the internal thermal noise effect becomes significant. In that case,  $\tilde{\mathbf{n}}_s^{m,T}(l) \approx \mathbf{G}^H \Phi_t^H \mathbf{B}_m \Phi_t \mathbf{v}_1(l)$ . Thus, the overall noise variance becomes  $\sigma_{n_s}^2 = \sigma_{n_s}^2 |(\Psi(n, n))|^2 \alpha_{\text{BS-RIS}} \left( \frac{\kappa}{1+\kappa} \sum_v |\mathbf{G}^{\text{LOS}}(n, v)|^2 + \frac{1}{1+\kappa} \right)$ , where  $\Psi = \Phi_t^H \mathbf{B}_m \Phi_t$  and  $v \in \{1, 2, \dots, T_x\}$ .<sup>1</sup>

Then, using (22), the overall received echo signal over the  $L$  time block is given as

$$\mathbf{Y}_s^{m,T} = \beta_{\text{RIS}}^{m,T} \mathbf{G}^H \Phi_t^H \mathbf{B}_m \Phi_t \mathbf{G} \mathbf{X} + \tilde{\mathbf{n}}_s^{m,T} \quad (23)$$

<sup>1</sup>For  $Z = XY$ , where  $X$  and  $Y$  are independent random variables, the distribution of  $Z$  is characterized by  $\mu_Z = \mu_X \mu_Y$  and  $\sigma_Z^2 = \sigma_X^2 \mu_Y^2 + \sigma_Y^2 \mu_X^2 + \mu_X^2 \mu_Y^2$ .

$$\gamma_{m,T} \leq \frac{(\beta_{\text{RIS}}^{m,T})^2 \text{Tr}(\bar{\mathbf{G}} \Phi_t \mathbf{B}_m \Phi_t^H)^2 \text{Tr}(\mathbf{R}_x)}{\sum_{j \neq m}^{M_R} \text{Tr}(\mathbf{f}_{j,R}^H \mathbf{f}_{j,R})^2 \text{Tr}(\mathbf{R}_x) + \sum_{\tilde{m} \neq m}^{M_T} (\beta_{\text{RIS}}^{\tilde{m},T})^2 \text{Tr}(\bar{\mathbf{G}} \Phi_t \mathbf{B}_{\tilde{m},T} \Phi_t^H)^2 \text{Tr}(\mathbf{R}_x) + \sigma_{\tilde{n}_s}^2} \quad (31)$$

$$\gamma_{m,T} \leq \frac{(\beta_{\text{RIS}}^{m,T})^2 \text{Tr}(\bar{\mathbf{B}}_{m,T} \Phi_t^H \mathbf{A} \Phi_t) \text{Tr}(\Phi_t \Phi_t^H) \text{Tr}(\mathbf{R}_x)}{\sum_{j \neq m}^{M_R} \text{Tr}(\mathbf{f}_{j,R}^H \mathbf{f}_{j,R})^2 \text{Tr}(\mathbf{R}_x) + \sum_{\tilde{m} \neq m}^{M_T} (\beta_{\text{RIS}}^{\tilde{m},T})^2 \text{Tr}(\bar{\mathbf{B}}_{\tilde{m},T}^H \Phi_t^H \mathbf{A} \Phi_t) \text{Tr}(\Phi_t \Phi_t^H) \text{Tr}(\mathbf{R}_x) + \sigma_{\tilde{n}_s}^2} \quad (32)$$

where  $\mathbf{Y}_s^{m,T} = [\mathbf{y}_s^{m,T}(1), \dots, \mathbf{y}_s^{m,T}(L)]$ ,  $\mathbf{X} = [\mathbf{x}(1), \dots, \mathbf{x}(L)]$  and  $\tilde{\mathbf{N}}_s^{m,T} = [\tilde{\mathbf{n}}_s^{m,T}(1), \dots, \tilde{\mathbf{n}}_s^{m,T}(L)]$ . In the proposed scheme, the active transmissive STAR-RIS elements are first employed to transmit BS signals to Side- $T$  and then reflect the echo signals of the remote targets back to the BS. Therefore, using (23), the overall power consumption of the active transmissive elements can be calculated as

$$P_{\text{RIS}} \geq \left\| \Phi_t^H \mathbf{B}_m \Phi_t \mathbf{G} \mathbf{x}(l) \right\|^2 + \left\| \Phi_t^H \mathbf{B}_m \Phi_t \mathbf{v}_1(l) \right\|^2 + \left\| \Phi_t^H \mathbf{v}_2(l) \right\|^2. \quad (24)$$

After some manipulations, (24) can be rewritten as

$$P_{\text{RIS}} \geq \text{Tr}(\Phi_t^H \mathbf{B}_m \Phi_t \mathbf{G} \mathbf{R}_x \mathbf{G}^H \Phi_t^H \mathbf{B}_m^H \Phi_t) + \sigma_{v_1}^2 \text{Tr}(\Phi_t^H \mathbf{B}_m \Phi_t \Phi_t^H \mathbf{B}_m^H \Phi_t) + \sigma_{v_2}^2 \text{Tr}(\Phi_t^H \Phi_t). \quad (25)$$

Furthermore, for the mono-static MIMO radar systems whose transmit and receive elements are co-located, the round-trip path loss is calculated as [23, 39]

$$\beta_m = \sqrt{\frac{\lambda^2 \Lambda}{(4\pi)^3 d^4}} \quad (26)$$

where  $\Lambda$  is the radar cross section (RCS) and  $d$  is the distance between MIMO radar and the sensing target. Therefore, in the proposed scenario, since the hybrid STAR-RIS can be considered as a mono-static MIMO radar [23], the path attenuation coefficient of  $\beta_{\text{RIS}}^{m,T}$  in (23) is calculated for the corresponding distance  $d = d_{\text{RIS-O}_{m,T}}$ .

Unlike the remote sensing targets, since the nearby sensing targets on Side- $R$  have both direct and indirect connections with the BS, similar to (17), the channel between BS and sensing target  $m$  on Side- $R$  ( $\mathbf{O}_{m,R}$ ),  $\mathbf{a}(\theta_{s,h}^{m,R}, \theta_{s,v}^{m,R}) \in \mathbb{C}^{1 \times T_x}$ , can be expressed as

$$\mathbf{a}(\theta_{s,h}^{m,R}, \theta_{s,v}^{m,R}) = [1, \dots, e^{j\eta_{\text{BS}}(T_x-1) \sin(\theta_{s,h}^{m,R}) \cos(\theta_{s,v}^{m,R})}] \quad (27)$$

where  $m \in \{1, \dots, M_R\}$ ,  $\theta_{s,h}^{m,R}$  and  $\theta_{s,v}^{m,R}$  are horizontal and vertical AoDs from BS towards target  $\mathbf{O}_{m,R}$ , respectively. Therefore, following (27) and (21) for  $i = R$ , the received echo signal collected at the BS from the target  $\mathbf{O}_{m,R}$  over the paths of BS  $\rightarrow \mathbf{O}_{m,R} \rightarrow$  BS and BS  $\rightarrow$  STAR-RIS  $\rightarrow \mathbf{O}_{m,R} \rightarrow$  STAR-RIS  $\rightarrow$  BS becomes [40]

$$\mathbf{y}_s^{m,R}(l) = \beta_{\text{BS}}^{m,R} (\mathbf{a}(\theta_{s,h}^{m,R}, \theta_{s,v}^{m,R}) + \tilde{\mathbf{b}}(\varphi_{s,h}^{m,R}, \varphi_{s,v}^{m,R}) \Phi_r \mathbf{G})^H \times (\mathbf{a}(\theta_{s,h}^{m,R}, \theta_{s,v}^{m,R}) + \tilde{\mathbf{b}}(\varphi_{s,h}^{m,R}, \varphi_{s,v}^{m,R}) \Phi_r \mathbf{G}) \mathbf{x}(l) + \mathbf{n}_s^{m,R}(l) \quad (28)$$

where  $\mathbf{n}_s^{m,R}$  is the AWGN matrix whose each entry is i.i.d and with  $\sim \mathcal{CN}(0, \sigma_{m,R}^2)$  distribution and  $\tilde{\mathbf{b}}(\varphi_{s,h}^{m,R}, \varphi_{s,v}^{m,R}) \in \mathbb{C}^{1 \times N} = \sqrt{\beta_{\text{RIS}}^{m,R} / \beta_{\text{BS}}^{m,R}} \mathbf{b}(\varphi_{s,h}^{m,R}, \varphi_{s,v}^{m,R})$  for  $\beta_{\text{BS}}^{m,R}$  and  $\beta_{\text{RIS}}^{m,R}$  being the round-trip path attenuation from the BS and hybrid STAR-RIS to the target  $\mathbf{O}_{m,R}$  calculated as in (26) for corresponding  $d = d_{\text{BS-O}_{m,R}}$  and  $d = d_{\text{RIS-O}_{m,R}}$ , respectively. Then, over the  $L$  time block, (28) can be rewritten as

$$\mathbf{Y}_s^{m,R} = \beta_{\text{BS}}^{m,R} (\mathbf{a}(\theta_{s,h}^{m,R}, \theta_{s,v}^{m,R}) + \tilde{\mathbf{b}}(\varphi_{s,h}^{m,R}, \varphi_{s,v}^{m,R}) \Phi_r \mathbf{G})^H \times (\mathbf{a}(\theta_{s,h}^{m,R}, \theta_{s,v}^{m,R}) + \tilde{\mathbf{b}}(\varphi_{s,h}^{m,R}, \varphi_{s,v}^{m,R}) \Phi_r \mathbf{G}) \mathbf{X} + \mathbf{N}_s^{m,R} \quad (29)$$

where  $\mathbf{Y}_s^{m,R} = [\mathbf{y}_s^{m,R}(1), \dots, \mathbf{y}_s^{m,R}(L)]$  and  $\mathbf{N}_s^{m,R} = [\mathbf{N}_s^{m,R}(1), \dots, \mathbf{N}_s^{m,R}(L)]$ .

### III. PERFORMANCE METRICS AND PROBLEM FORMULATION

In this section, for the proposed system, an optimization problem that maximizes SINR of the sensing targets is formulated by optimizing transmissive/reflective coefficients of the hybrid STAR-RIS and beamforming matrix. Then, to evaluate sensing performance, SINR and CRB estimation of the sensing targets are derived.

#### A. Target SINR Analysis

In this subsection, the performance of the target SINR is determined.

For the remote targets on the Side- $T$  that perceive transmit signals through the active transmissive STAR-RIS elements, the target SINR can be given, considering interference from the other sensing targets both on Side- $R$  and Side- $T$ , as

$$\gamma_{m,T} = \frac{\left\| \beta_{\text{RIS}}^{m,T} \mathbf{G}^H \Phi_t^H \mathbf{B}_m \Phi_t \mathbf{G} \mathbf{X} \right\|^2}{\sum_{j=1}^{M_R} \left\| \mathbf{f}_{j,R}^H \mathbf{f}_{j,R} \mathbf{X} \right\|^2 + \sum_{\tilde{m} \neq m}^{M_T} \left\| \beta_{\text{RIS}}^{\tilde{m},T} \mathbf{G}^H \Phi_t^H \mathbf{B}_{\tilde{m},T} \Phi_t \mathbf{G} \mathbf{X} \right\|^2 + \sigma_{m,T}^2} \quad (30)$$

where  $\mathbf{f}_{j,R} = \beta_{\text{BS}}^{j,R} (\mathbf{a}(\theta_{s,h}^{j,R}, \theta_{s,v}^{j,R}) + \tilde{\mathbf{b}}(\varphi_{s,h}^{j,R}, \varphi_{s,v}^{j,R}) \Phi_r \mathbf{G})$ . After some simplification<sup>2</sup>, (30) can be rewritten as in (31) for  $\bar{\mathbf{G}} = \mathbf{G}^H \mathbf{G}$  at the beginning of the this page.

Here, employing Cauchy Schwartz inequality [41] for  $\text{Tr}(\mathbf{K}\mathbf{L})^2 \leq \text{Tr}(\mathbf{K}^H \mathbf{K}) \text{Tr}(\mathbf{L}^H \mathbf{L})$ , the target SINR of  $\mathbf{O}_{m,B}$  in (31) is upper bounded as in (32). Then, using [41, Theorem

<sup>2</sup>For  $\mathbf{K}$ ,  $\mathbf{L}$  and  $\mathbf{M}$  being matrices with coherent dimensions, the trace of matrix product is  $\text{Tr}(\mathbf{K}\mathbf{L}\mathbf{M}) = \text{Tr}(\mathbf{M}\mathbf{K}\mathbf{L}) = \text{Tr}(\mathbf{L}\mathbf{M}\mathbf{K})$  [41].

$$\gamma_{m,T} \leq \frac{P_A(\beta_{\text{RIS}}^{m,T})^2 \text{Tr}(\mathbf{Q}_{m,T}\mathbf{Z}_t) \text{Tr}(\mathbf{R}_x)}{\sum_{j \neq m}^{M_R} \text{Tr}((\mathbf{f}_{j,R}^H \mathbf{f}_{j,R})^2) \text{Tr}(\mathbf{R}_x) + \sum_{\tilde{m} \neq m}^{M_T} P_A(\beta_{\text{RIS}}^{\tilde{m},T})^2 \text{Tr}(\mathbf{Q}_{\tilde{m},T}\mathbf{Z}_t) \text{Tr}(\mathbf{R}_x) + \sigma_{n_s}^2} \quad (33)$$

$$\gamma_{m,R} \leq \frac{(\beta_{\text{BS}}^{m,R})^2 \text{Tr}(\mathbf{R}_x) (\text{Tr}(\mathbf{A}_m \mathbf{A}_m^H) + N \text{Tr}(\mathbf{Q}_{m,R}\mathbf{Z}_r))}{\sum_{\tilde{m} \neq m}^{M_R} (\beta_{\text{BS}}^{\tilde{m},R})^2 \text{Tr}(\mathbf{R}_x) ((\text{Tr}(\mathbf{A}_{\tilde{m},R} \mathbf{A}_{\tilde{m},R}^H) + N \text{Tr}(\mathbf{Q}_{\tilde{m},R}\mathbf{Z}_r)) + \sum_{j=1}^{M_T} P_A(\beta_{\text{RIS}}^{j,T})^2 \text{Tr}(\mathbf{Q}_{j,T}\mathbf{Z}_t) \text{Tr}(\mathbf{R}_x) + \sigma_{n_s}^2} \quad (34)$$

1.10], for  $\mathbf{Q}_{m,T} \in \mathbb{C}^{N \times N} = \mathbf{B}_m \mathbf{B}_m^H \odot \bar{\mathbf{G}}^H \bar{\mathbf{G}}$ ,  $\mathbf{Q}_{\tilde{m},T} \in \mathbb{C}^{N \times N} = \mathbf{B}_{\tilde{m}} \mathbf{B}_{\tilde{m}}^H \odot \bar{\mathbf{G}}^H \bar{\mathbf{G}}$  and  $\mathbf{Z}_t \in \mathbb{C}^{N \times N} = \mathbf{z}_t^H \mathbf{z}_t$  for  $\mathbf{z}_t \in \mathbb{C}^{1 \times N} = [\xi_{t,1} e^{j\phi_{t,1}}, \xi_{t,2} e^{j\phi_{t,2}}, \dots, \xi_{t,N} e^{j\phi_{t,N}}]$ , the target SINR in (32) can be bounded as in (33).

Similarly, considering the received echo signal given in (29), for  $\text{Tr}(\Phi_r^H \Phi_r) = N$  and using  $\text{Tr}((\mathbf{K} + \mathbf{L})(\mathbf{K} + \mathbf{L})^H) \leq 2(\text{Tr}(\mathbf{K}\mathbf{K}^H) + \text{Tr}(\mathbf{L}\mathbf{L}^H))$  [41], the target SINR of each  $\mathbf{O}_{m,R}$  can be upper bounded as in (34), where  $\mathbf{A}_m \in \mathbb{C}^{T_x \times T_x} = \mathbf{a}(\theta_{s,h}^{m,R}, \theta_{s,v}^{m,R}) \mathbf{a}^H(\theta_{s,h}^{m,R}, \theta_{s,v}^{m,R})$ ,  $\mathbf{Q}_{m,R} \in \mathbb{C}^{N \times N} = \tilde{\mathbf{B}}_m \tilde{\mathbf{B}}_m^H \odot \bar{\mathbf{G}}^H \bar{\mathbf{G}}$ ,  $\tilde{\mathbf{B}}_m \in \mathbb{C}^{N \times N} = \tilde{\mathbf{b}}(\varphi_{s,h}^{m,R}, \varphi_{s,v}^{m,R}) \tilde{\mathbf{b}}^H(\varphi_{s,h}^{m,R}, \varphi_{s,v}^{m,R})$ ,  $\mathbf{Z}_r \in \mathbb{C}^{N \times N} = \mathbf{z}_r^H \mathbf{z}_r$ ,  $\mathbf{z}_r \in \mathbb{C}^{1 \times N} = [e^{j\phi_{r,1}}, e^{j\phi_{r,2}}, \dots, e^{j\phi_{r,N}}]$  and  $j \in \{1, \dots, M_T\}$ .

## B. Problem Formulation

To optimize the coefficients of the hybrid STAR-RIS the following optimization problem is formulated that maximizes the sum of the target SINR as follows

$$(P1) \quad \max_{\Phi_t, \Phi_r} \sum_{i \in \mathcal{S}} \sum_{m=1}^{M_i} \gamma_{m,i} \quad (35a)$$

$$\text{s.t.} \quad |\mathbf{z}_r(n)| = 1, \quad \forall n \in \{1, \dots, N\} \quad (35b)$$

$$|\mathbf{z}_t(n)| \geq 1, \quad \forall n \in \{1, \dots, N\} \quad (35c)$$

$$\text{Tr}(\mathbf{R}_x) \leq P_{\text{BS}} \quad (35d)$$

$$\text{Tr}(\mathbf{Z}_t) \leq P_A \quad (35e)$$

Here, the problem (P1) is converted to a standard SDP-based problem assuming  $\text{Tr}(\mathbf{R}_x) \approx P_{\text{BS}}$  as follows

$$(P2) \quad \sum_{i \in \mathcal{S}} \sum_{m=1}^{M_i} f_i(m) - \hat{f}_i(m) \quad (36)$$

$$\text{s.t.} \quad f_i(m) - \hat{f}_i(m) \geq 0$$

$$(35b-35e)$$

where  $f_T(m) = P_A(\beta_{\text{RIS}}^{m,T})^2 P_{\text{BS}} \text{Tr}(\mathbf{Q}_{m,T}\mathbf{Z}_t)$  and  $\hat{f}_T(m) = \sum_{j \neq m}^{M_R} \text{Tr}(\mathbf{f}_{j,R}^H \mathbf{f}_{j,R})^2 P_{\text{BS}} + \sum_{\tilde{m} \neq m}^{M_T} P_A(\beta_{\text{RIS}}^{\tilde{m},T})^2 \text{Tr}(\mathbf{Q}_{\tilde{m},T}\mathbf{Z}_t) \text{Tr}(\mathbf{R}_x) + \sigma_{m,T}^2$ , while  $f_R(m) = (\beta_{\text{BS}}^{m,R})^2 P_{\text{BS}} (\text{Tr}(\mathbf{A}_m \mathbf{A}_m^H) + N \text{Tr}(\mathbf{Q}_{m,R}\mathbf{Z}_r))$  and  $\hat{f}_R(m) = \sum_{\tilde{m} \neq m}^{M_R} (\beta_{\text{BS}}^{\tilde{m},R})^2 P_{\text{BS}} ((\text{Tr}(\mathbf{A}_{\tilde{m},R} \mathbf{A}_{\tilde{m},R}^H) + N \text{Tr}(\mathbf{Q}_{\tilde{m},R}\mathbf{Z}_r)) + \sum_{j=1}^{M_T} P_A(\beta_{\text{RIS}}^{j,T})^2 P_{\text{BS}} \text{Tr}(\mathbf{Q}_{j,T}\mathbf{Z}_t) + \sigma_{j,R}^2$ .

Here, the optimization problem (P2) can be efficiently solved with CVX solvers [28]. Then the beamforming matrix is determined using optimal transmit beamforming

via defining the overall beamforming matrix in (6) as  $\mathbf{W} \in \mathbb{C}^{T_x \times (K+M)} = [\mathbf{w}_{c,1}, \dots, \mathbf{w}_{c,K}, \mathbf{w}_{s,1}, \dots, \mathbf{w}_{s,M}]$ . Here,  $\mathbf{w}_{c,p}$  and  $\mathbf{w}_{s,q}$  are the beamforming vectors corresponding to  $p$ -th communication user and  $q$ -th sensing target, respectively. These beamforming vectors are defined as follows

$$\mathbf{w}_{c,p} = \sqrt{P_c} \frac{\tilde{\mathbf{h}}_{c,p}}{\|\tilde{\mathbf{h}}_{c,p}\|}, \quad \mathbf{w}_{s,q} = \sqrt{P_s} \frac{\tilde{\mathbf{h}}_{s,q}}{\|\tilde{\mathbf{h}}_{s,q}\|} \quad (37)$$

where  $\tilde{\mathbf{h}}_{c,p}$  is the overall channel for the  $p$ -th communication user and  $\tilde{\mathbf{h}}_{s,q}$  is the overall channel for  $q$ -th sensing target. Here, for a communication user on Side- $T$ ,  $\tilde{\mathbf{h}}_{c,p} = \mathbf{h}_{k,T} \Phi_t \mathbf{G}$  (19), while for those on Side- $R$ , it is  $\tilde{\mathbf{h}}_{c,p} = \mathbf{h}_{k,R} \Phi_r \mathbf{G} + \mathbf{g}_{k,R}$  (20). Similarly, for a sensing target on Side- $T$  (22),  $\tilde{\mathbf{h}}_{s,q} = \mathbf{b}(\varphi_{s,h}^{m,T}, \varphi_{s,v}^{m,T}) \Phi_t \mathbf{G}$ , while for ones on Side- $R$  (20), it is  $\tilde{\mathbf{h}}_{s,q} = \mathbf{a}(\theta_{s,h}^{m,R}, \theta_{s,v}^{m,R}) + \tilde{\mathbf{b}}(\varphi_{s,h}^{m,R}, \varphi_{s,v}^{m,R}) \Phi_r \mathbf{G}$ . Additionally, the transmit power for each communication user and sensing target is represented as  $P_c$  and  $P_s$ , respectively, where  $P_c = P_s = P_{\text{BS}}/(K+M)$ .

## C. Cramer-Rao Bound (CRB) Analysis

In this section, to evaluate sensing performance of the targets, the CRB estimation for 2D AoDs of the targets has been investigated. To achieve this, first, the Fisher information matrix (FIM) is derived.

Let  $\zeta_{m,i} \in \mathbb{C}^{4 \times 1} = [\varphi^{m,i}, \beta^{m,i}]^T$  be the vector of unknown parameters to be estimated that includes 2D AoDs of  $m$ th target on Side- $i$ ,  $\varphi^{m,i} \in \mathbb{C}^{1 \times 2}$  and its corresponding complex channel coefficient  $\beta^{m,i} \in \mathbb{C}^{1 \times 2}$ , where  $i \in \mathcal{S} = \{T, R\}$  and  $m \in \{1, \dots, M_i\}$ . For the remote target on the Side- $T$ ,  $\varphi^{m,T} = [\varphi_{s,h}^{m,T}, \varphi_{s,v}^{m,T}]$  and complex channel coefficient  $\beta^{m,T} = [\Re(\beta_{\text{RIS}}^{m,T}), \Im(\beta_{\text{RIS}}^{m,T})]$ . Then, in order to obtain the FIM, overall received echo signal in (23) is vectorized for  $\mathbf{u}_{m,T} = \beta_{\text{RIS}}^{m,T} \text{vec}(\mathbf{G}^H \Phi_t^H \mathbf{B}_m \Phi_t \mathbf{G} \mathbf{X})$ ,  $\tilde{\mathbf{n}}_{m,T} = \text{vec}(\tilde{\mathbf{N}}_s^{m,T})$  as follows

$$\mathbf{y}_s^{m,T} = \mathbf{u}_{m,T} + \tilde{\mathbf{n}}_{m,T}. \quad (38)$$

Therefore, the FIM for estimating  $\zeta_{m,T}$  is constructed as [42]

$$\mathbf{J}_{m,T} = \begin{bmatrix} \mathbf{J}_{\varphi\varphi}^{m,T} & \mathbf{J}_{\varphi\beta}^{m,T} \\ \mathbf{J}_{\beta\varphi}^{m,T} & \mathbf{J}_{\beta\beta}^{m,T} \end{bmatrix}. \quad (39)$$

Then, utilizing (39), the CRB can be expressed as [42]

$$\text{CRB}(\varphi_{m,T}) = [\mathbf{J}_{\varphi\varphi}^{m,T} - \mathbf{J}_{\varphi\beta}^{m,T} (\mathbf{J}_{\beta\beta}^{m,T})^{-1} \mathbf{J}_{\beta\varphi}^{m,T}]^{-1} \quad (40)$$

where

$$\mathbf{J}_{m,T}(p, q) = \frac{2}{\sigma_{n_s}^2} \Re \left\{ \frac{\partial \mathbf{u}_{m,T}^H}{\partial \zeta_p} \frac{\partial \mathbf{u}_{m,T}}{\partial \zeta_q} \right\} \quad p, q \in \{1, 2, 3, 4\} \quad (41)$$

Here,  $\mathbf{B}_m = \mathbf{b}^H(\varphi_{s,h}^{m,T}, \varphi_{s,v}^{m,T}) \mathbf{b}(\varphi_{s,h}^{m,T}, \varphi_{s,v}^{m,T})$

$$\frac{\partial \mathbf{u}_{m,T}}{\partial \varphi_{m,T}} = \left[ \beta_{\text{RIS}}^{m,T} \text{vec}(\mathbf{G}^H \Phi_t^H \dot{\mathbf{B}}_{\varphi_h}^m \Phi_t \mathbf{G} \mathbf{X}), \beta_{\text{RIS}}^{m,T} \text{vec}(\mathbf{G}^H \Phi_t^H \dot{\mathbf{B}}_{\varphi_v}^m \Phi_t \mathbf{G} \mathbf{X}) \right] \quad (42)$$

$$\frac{\partial \mathbf{u}_{m,T}}{\partial \beta_{m,T}} = \text{vec}(\mathbf{G}^H \Phi_t^H \mathbf{B}_m \Phi_t \mathbf{G} \mathbf{X}) [1 \ j] \quad (43)$$

where  $\dot{\mathbf{B}}_{\varphi_h}^m = \frac{\partial \mathbf{B}_m}{\partial \varphi_{s,h}^{m,T}}$  and  $\dot{\mathbf{B}}_{\varphi_v}^m = \frac{\partial \mathbf{B}_m}{\partial \varphi_{s,v}^{m,T}}$ . Therefore, since  $\mathbf{b}(\varphi_{s,h}^{m,T}, \varphi_{s,v}^{m,T}) = e^{j\eta_{\text{RIS}}} (\mathbf{k}_x \sin(\varphi_{s,h}^{m,T}) \cos(\varphi_{s,v}^{m,T}) + \mathbf{k}_y \sin(\varphi_{s,h}^{m,T}) \sin(\varphi_{s,v}^{m,T}))$  as expressed in (16), where  $\mathbf{k}_x$  and  $\mathbf{k}_y$  are vectors with scalar elements,  $\dot{\mathbf{B}}_{\varphi_h}^m$  and  $\dot{\mathbf{B}}_{\varphi_v}^m$  can be calculated as

$$\dot{\mathbf{B}}_{\varphi_h} = j\eta_{\text{RIS}} (\mathbf{k}_x^H \cos(\varphi_{s,h}^{m,T}) \cos(\varphi_{s,v}^{m,T}) + \mathbf{k}_y^H \cos(\varphi_{s,h}^{m,T}) \sin(\varphi_{s,v}^{m,T})) \times (-\mathbf{b}(\varphi_{s,h}^{m,T}, \varphi_{s,v}^{m,T})^H \mathbf{b}(\varphi_{s,h}^{m,T}, \varphi_{s,v}^{m,T}) + \mathbf{b}(\varphi_{s,h}^{m,T}, \varphi_{s,v}^{m,T}) \mathbf{b}(\varphi_{s,h}^{m,T}, \varphi_{s,v}^{m,T})^H) \quad (44)$$

$$\dot{\mathbf{B}}_{\varphi_v} = j\eta_{\text{RIS}} (-\mathbf{k}_x^H \sin(\varphi_{s,h}^{m,T}) \sin(\varphi_{s,v}^{m,T}) + \mathbf{k}_y^H \sin(\varphi_{s,h}^{m,T}) \cos(\varphi_{s,v}^{m,T})) \times (-\mathbf{b}(\varphi_{s,h}^{m,T}, \varphi_{s,v}^{m,T})^H \mathbf{b}(\varphi_{s,h}^{m,T}, \varphi_{s,v}^{m,T}) + \mathbf{b}(\varphi_{s,h}^{m,T}, \varphi_{s,v}^{m,T}) \mathbf{b}(\varphi_{s,h}^{m,T}, \varphi_{s,v}^{m,T})^H) \quad (45)$$

Let the overall signal be represented as  $\mathbf{F}_m = \mathbf{G}^H \Phi_t^H \mathbf{B}_m \Phi_t \mathbf{G} \mathbf{X}$ , while  $\dot{\mathbf{F}}_{\varphi_h} = \mathbf{G}^H \Phi_t^H \dot{\mathbf{B}}_{\varphi_h}^m \Phi_t \mathbf{G} \mathbf{X}$  and  $\dot{\mathbf{F}}_{\varphi_v} = \mathbf{G}^H \Phi_t^H \dot{\mathbf{B}}_{\varphi_v}^m \Phi_t \mathbf{G} \mathbf{X}$ . Therefore, the elements of the FIM can be defined as [19]

$$\mathbf{J}_{\varphi\varphi}^{m,T}(\mathbf{F}_m) = \frac{2L}{\sigma_{n_s}^2} (\beta_{\text{RIS}}^{m,T})^2 \Re \left\{ \begin{bmatrix} \text{Tr}(\dot{\mathbf{F}}_{\varphi_h} \mathbf{R}_x \dot{\mathbf{F}}_{\varphi_h}^H) & \text{Tr}(\dot{\mathbf{F}}_{\varphi_h} \mathbf{R}_x \dot{\mathbf{F}}_{\varphi_v}^H) \\ \text{Tr}(\dot{\mathbf{F}}_{\varphi_v} \mathbf{R}_x \dot{\mathbf{F}}_{\varphi_h}^H) & \text{Tr}(\dot{\mathbf{F}}_{\varphi_v} \mathbf{R}_x \dot{\mathbf{F}}_{\varphi_v}^H) \end{bmatrix} \right\} \quad (46)$$

$$\mathbf{J}_{\varphi\beta}^{m,T}(\mathbf{F}_m) = \frac{2L}{\sigma_{n_s}^2} \Re \left\{ \begin{bmatrix} \beta_{\text{RIS}}^{m,T} \text{Tr}(\mathbf{F}_m \mathbf{R}_x \dot{\mathbf{F}}_{\varphi_h}^H) \\ \beta_{\text{RIS}}^{m,T} \text{Tr}(\mathbf{F}_m \mathbf{R}_x \dot{\mathbf{F}}_{\varphi_v}^H) \end{bmatrix} \begin{bmatrix} 1 \\ j \end{bmatrix} \right\} \quad (47)$$

$$\mathbf{J}_{\beta\beta}^{m,T}(\mathbf{F}_m) = \frac{2L}{\sigma_{n_s}^2} \mathbf{I}_2 \text{Tr}(\mathbf{F}_m \mathbf{R}_x \mathbf{F}_m^H) \quad (48)$$

Then, the CRB of the  $m$ th remote target is obtained by substituting (46-48) into (40).

In similar way, the CRB of the sensing targets on Side- $R$  can be calculated for AoDs from BS to the target  $\mathbf{O}_{m,R}$ ,  $\theta^{m,R} = [\theta_{s,h}^{m,R}, \theta_{s,v}^{m,R}]$  and complex channel coefficient  $\beta^{m,R} = [\Re(\beta_{\text{BS}}^{m,R}), \Im(\beta_{\text{BS}}^{m,R})]$  via following (40-48) steps.

#### IV. SIMULATION RESULTS

In this section, Monte Carlo simulation results are provided to evaluate the sensing performance of the hybrid STAR-RIS-assisted ISAC scheme and the proposed optimization algorithm. Computer simulation results are conducted for a two-user and two-target scenario, where there is one user and

TABLE I  
SYSTEM PARAMETERS

Notation	Parameter	Value
$f_c$	Operating frequency	3.315 GHz
$T_x$	Number of transmit/receive antennas at BS	8
$K$	Total number of communication users	2
$M$	Total number of sensing targets	2
$\kappa$	Rician factor	3 dB
$\sigma_{n_s}^2 = \sigma_{n_c}^2$	Noise power	-80 dBm
$L$	Coherence time length	100
$\alpha_0$	Reference path loss at 1 m	30 dB
$\rho$	Path loss exponent	2.2
$\Lambda$	RCS	100 m <sup>2</sup>
$\theta_h^R, \theta_v^R$	AoDs of target $\mathbf{O}_R$	{35°, 110°}
$\varphi_h^T, \varphi_v^T$	AoDs of target $\mathbf{O}_T$	{40°, 108°}
$d_{\text{BS-RIS}}$	Distance: BS-STAR-RIS	5 m
$d_{\text{RIS-O}_T}, d_{\text{RIS-U}_T}$	Distances: RIS- $\mathbf{O}_T$ and RIS- $\mathbf{U}_T$	{17, 18} m
$d_{\text{BS-O}_R}, d_{\text{RIS-O}_R}$	Distances: BS- $\mathbf{O}_R$ and STAR-RIS- $\mathbf{O}_R$	{38, 41} m
$d_{\text{BS-U}_R}, d_{\text{RIS-U}_R}$	Distances: BS- $\mathbf{U}_R$ and STAR-RIS- $\mathbf{U}_R$	{25, 27} m

one target located on each side ( $T, R$ ) of the hybrid STAR-RIS. Specifically, the user and target at Side- $R$  denoted as  $\mathbf{U}_R$  and  $\mathbf{O}_R$ , while those on Side- $T$  are referred to as  $\mathbf{U}_T$  and  $\mathbf{O}_T$ , respectively. Additionally, system parameters used in the simulations are listed in Table I.

Fig. 2 presents the SINR of the target on Side- $T$ , denoted as  $\mathbf{O}_T$ , for  $N = 36$  hybrid STAR-RIS elements with varying transmit power levels at the BS,  $P_{\text{BS}} = \{10, 15, 20, 25\}$  dB. The results clearly show that increasing  $P_{\text{BS}}$  enhances the SINR performance of the target  $\mathbf{O}_T$ . However, higher  $P_{\text{BS}}$  values also lead to greater power consumption of the active transmissive elements at the STAR-RIS, as discussed in (25). This indicates a fundamental trade-off between improving SINR and increasing power consumption of the active STAR-RIS elements that is crucial for ensuring efficiency of the overall system performance. Additionally, it can be deduced from Fig. 2 that after a certain  $P_{\text{RIS}}$  value, the increased thermal noise from the active transmissive elements causes the target SINR values to saturate. This further supports that remaining at lower  $P_{\text{RIS}}$  range is significant for maintaining efficient target SINR performance.

In Fig. 3, the SINR of the target on Side- $R$ , denoted as  $\mathbf{O}_R$ , is given for  $N = 36$  and different  $P_{\text{BS}}$  values. The results indicate a degradation in SINR of the target with increasing  $P_{\text{RIS}}$ . This degradation can be attributed to the active transmissive elements utilized for serving the remote target  $\mathbf{O}_T$ , which introduce interference for  $\mathbf{O}_R$ , as described in (34). Therefore, since the increasing the power of the those active elements enhances the interference for  $\mathbf{O}_R$ , which in turn leads to a reduction in the SINR of the target  $\mathbf{O}_R$ . On the other hand,

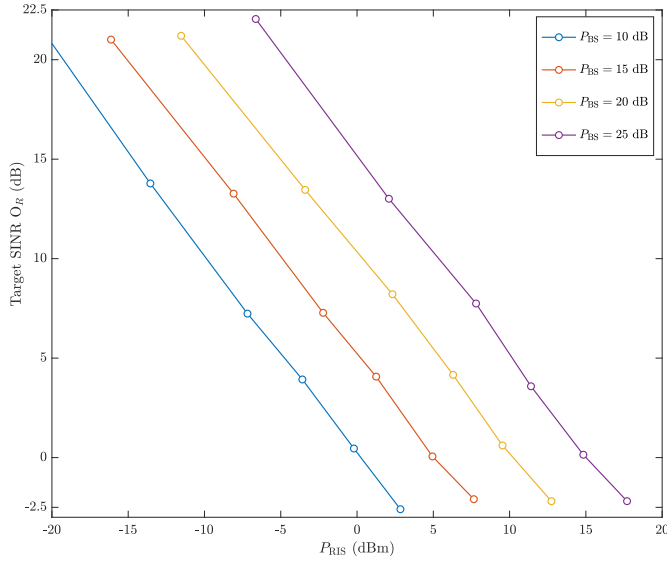


Fig. 2. SINR of target  $O_T$  versus power consumption at active STAR-RIS elements for  $N = 36$  and different  $P_{BS}$  values.

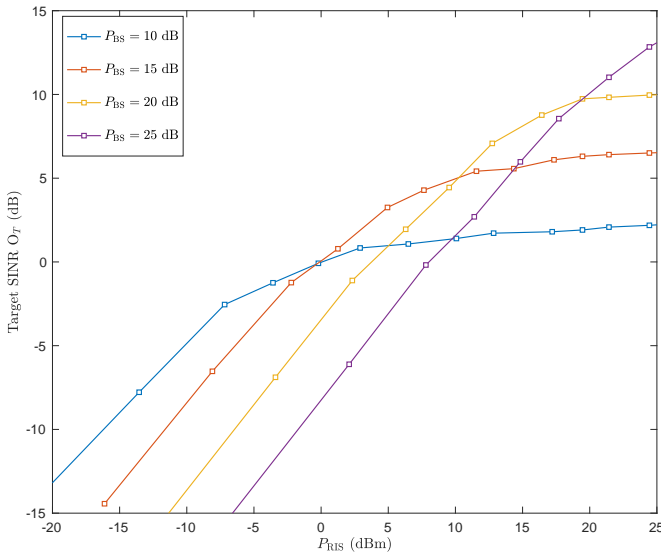


Fig. 3. SINR of target  $O_R$  versus power consumption at active STAR-RIS elements for  $N = 36$  and different  $P_{BS}$  values.

when  $P_{RIS}$  is held constant, an improvement in the SINR of the target  $O_R$  is also observed with increasing  $P_{BS}$  values. Notably, it is obvious that there is an approximate 5 dB improvement in the target SINR of  $O_R$  for every 5 dB increment in  $P_{BS}$ .

Fig. 4 presents the SINR performance of the targets  $O_R$  and  $O_T$  for increasing numbers of hybrid STAR-RIS elements  $N$ . When  $P_{BS}$  remains constant, a considerable improvement in SINR of the target  $O_T$  and a degradation in the SINR of the target  $O_R$  is observed with increasing  $N$ . Moreover, the results also indicate that after reaching certain values of  $P_{BS}$ , the changes in SINR performance for both targets become minimal. A possible explanation for this might be the SINR performance of the targets stabilizes due to a balance between their signal and interference powers. Furthermore, the results

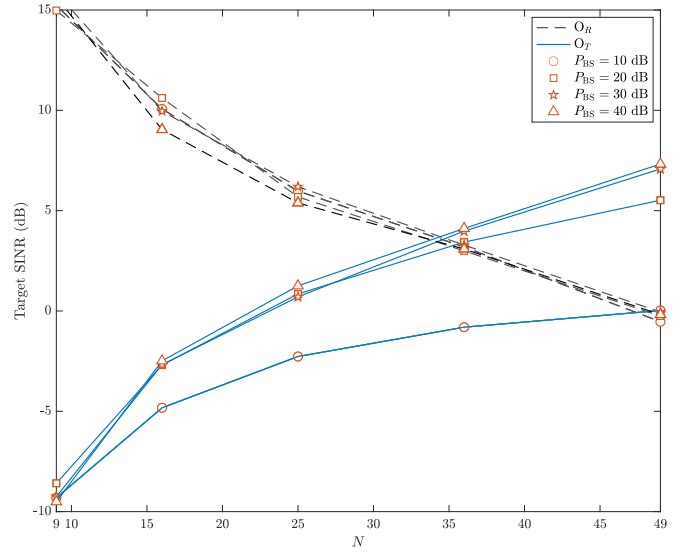


Fig. 4. SINR of the targets  $O_R$  and  $O_T$  for varying numbers of hybrid STAR-RIS elements  $N$ .

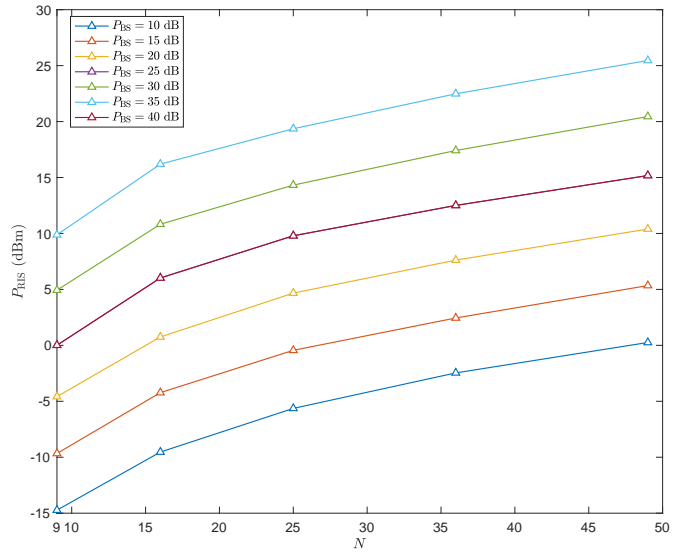


Fig. 5. Power consumption of active transmissive elements  $P_{RIS}$  versus  $N$  for varying  $P_{BS}$ .

suggest a fair SINR distribution between the targets on both sides for different  $N$  values. Specifically, the SINR of target  $O_R$  and target  $O_T$  reach almost an equilibrium with  $N = 36$  at  $P_{RIS} = 20, 30, 40$  dB, while achieving a balanced SINR at  $P_{BS} = 10$  dB requires  $N = 49$ .

In Fig. 5, the power consumption of active transmissive elements  $P_{RIS}$  is given for varying numbers of hybrid STAR-RIS elements  $N$ . As corroborated by (25) and the results presented in Figs. 2-4 is obvious that an increase in  $N$  leads to higher  $P_{RIS}$ . Particularly, for a certain  $N$  value, a 5 dB increase in  $P_{BS}$  results in 5 dBm increase in  $P_{RIS}$ .

In Fig. 6, the root CRB estimation of 2D AoDs of the target  $O_T$  is given for and different  $N$  values at  $P_{BS} = 20$  dB. Here, as  $N$  increases, there is a noticeable improvement in the root



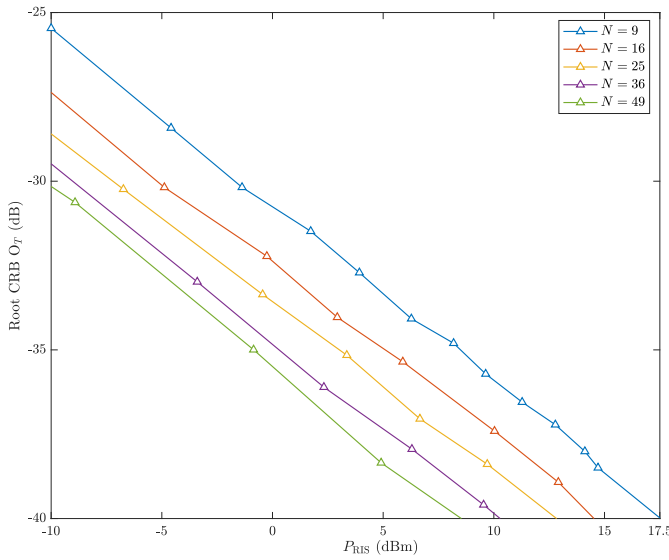


Fig. 6. Root CRB of target  $O_T$  versus power consumption of active transmissive elements  $P_{RIS}$  for varying numbers of hybrid STAR-RIS elements  $N$ .

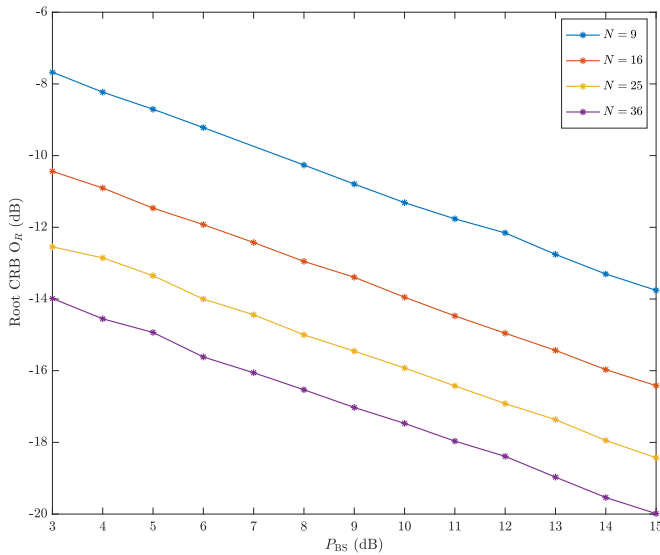


Fig. 7. Root CRB of target  $O_R$  versus  $P_{BS}$  for varying numbers of hybrid STAR-RIS elements  $N$ .

CRB estimation. This can be attributed to enhanced sensing signal power and an accompanying rise in  $P_{RIS}$  as  $N$  increases. It can be also observed that to achieve an improved root CRB value, the hybrid STAR-RIS with lower  $N$  elements requires a considerably a higher power consumption  $P_{RIS}$ . This implies that a hybrid STAR-RIS with a lower numbers of elements  $N$  necessitates a higher amplification factor  $P_A$ .

In Fig. 7, the root CRB estimation for AoDs of the target  $O_R$  is given for varying  $P_{BS}$ . It is apparent from the results that an increase in  $P_{BS}$  and  $N$  improve the CRB estimation of AoDs of the target  $O_R$ . It is also observed that when root CRB is kept constant, a hybrid STAR-RIS comprising a higher number of  $N$  elements necessitate a lower  $P_{BS}$  at the BS.

## V. CONCLUSION

This paper has proposed a novel hybrid STAR-RIS-aided ISAC transmission scheme with full-space communication and sensing capabilities for multi-user and multi-target scenarios. In the proposed scheme, to address significant path attenuation resulting from multi-hop transmission, low-power active transmissive elements have been considered at the hybrid STAR-RIS that introduce considerable power consumption. Moreover, sensing performance metrics including target SINR and CRB for 2D AoDs estimation have been derived. An SDR-based optimization algorithm has been developed to maximize the sum of SINR of the targets by optimizing transmissive and reflective coefficients of the hybrid STAR-RIS elements. Furthermore, to evaluate sensing performance of the system and illustrate the effectiveness of the proposed algorithm, a comprehensive simulations have been conducted.

## REFERENCES

- [1] Recommendation ITU-R M.2160-0, "Framework and overall objectives of the future development of IMT for 2030 and beyond," Tech. Rep., Nov. 2023.
- [2] F. Liu, Y. Cui, C. Masouros, J. Xu, T. X. Han, Y. C. Eldar, and S. Buzzi, "Integrated sensing and communications: Toward dual-functional wireless networks for 6G and beyond," *IEEE J. Sel. Areas Commun.*, vol. 40, no. 6, pp. 1728–1767, Mar. 2022.
- [3] Y. Cui, F. Liu, X. Jing, and J. Mu, "Integrating sensing and communications for ubiquitous IoT: Applications, trends, and challenges," *IEEE Netw.*, vol. 35, no. 5, pp. 158–167, Nov. 2021.
- [4] F. Liu, C. Masouros, A. P. Petropulu, H. Griffiths, and L. Hanzo, "Joint radar and communication design: Applications, state-of-the-art, and the road ahead," *IEEE Trans. Commun.*, vol. 68, no. 6, pp. 3834–3862, Feb. 2020.
- [5] J. A. Zhang, F. Liu, C. Masouros, R. W. Heath, Z. Feng, L. Zheng, and A. Petropulu, "An overview of signal processing techniques for joint communication and radar sensing," *IEEE J. Sel. Topics Signal Process.*, vol. 15, no. 6, pp. 1295–1315, Sep. 2021.
- [6] A. Hassanien, M. G. Amin, Y. D. Zhang, and F. Ahmad, "Signaling strategies for dual-function radar communications: An overview," *IEEE Aerosp. Electron. Syst. Mag.*, vol. 31, no. 10, pp. 36–45, Oct. 2016.
- [7] E. Basar, M. Di Renzo, J. De Rosny, M. Debbah, M.-S. Alouini, and R. Zhang, "Wireless communications through reconfigurable intelligent surfaces," *IEEE Access*, vol. 7, pp. 116 753–116 773, Aug. 2019.
- [8] E. Basar, G. C. Alexandropoulos, Y. Liu, Q. Wu, S. Jin, C. Yuen, O. A. Dobre, and R. Schober, "Reconfigurable intelligent surfaces for 6G: Emerging hardware architectures, applications, and open challenges," *IEEE Veh. Technol. Mag. (to appear)*, June 2024.
- [9] M. Di Renzo, A. Zappone, M. Debbah, M.-S. Alouini, C. Yuen, J. De Rosny, and S. Tretyakov, "Smart radio environments empowered by reconfigurable intelligent surfaces: How it works, state of research, and the road ahead," *IEEE J. Sel. Areas Commun.*, vol. 38, no. 11, pp. 2450–2525, July 2020.
- [10] Q. Wu, B. Zheng, C. You, L. Zhu, K. Shen, X. Shao, W. Mei, B. Di, H. Zhang, E. Basar *et al.*, "Intelligent surfaces empowered wireless network: Recent advances and the road to 6G," *Proc. IEEE (Early Access)*, Apr. 2024.
- [11] C. Huang, A. Zappone, G. C. Alexandropoulos, M. Debbah, and C. Yuen, "Reconfigurable intelligent surfaces for energy efficiency in wireless communication," *IEEE Trans. Wireless Commun.*, vol. 18, no. 8, pp. 4157–4170, June 2019.
- [12] E. Basar, "Transmission through large intelligent surfaces: A new frontier in wireless communications," in *2019 European Conference on Networks and Communications (EuCNC)*. IEEE, June 2019, pp. 112–117.
- [13] S. Zhang and R. Zhang, "Capacity characterization for intelligent reflecting surface aided MIMO communication," *IEEE J. Sel. Areas Commun.*, vol. 38, no. 8, pp. 1823–1838, June 2020.
- [14] Q. Wu and R. Zhang, "Intelligent reflecting surface enhanced wireless network via joint active and passive beamforming," *IEEE Trans. Wireless Commun.*, vol. 18, no. 11, pp. 5394–5409, Aug. 2019.

- [15] J. Chen, Y.-C. Liang, Y. Pei, and H. Guo, "Intelligent reflecting surface: A programmable wireless environment for physical layer security," *IEEE Access*, vol. 7, pp. 82 599–82 612, June 2019.
- [16] A. M. Elbir, K. V. Mishra, M. B. Shankar, and S. Chatzinotas, "The rise of intelligent reflecting surfaces in integrated sensing and communications paradigms," *IEEE Netw.*, vol. 37, no. 6, pp. 224–231, Dec. 2022.
- [17] R. Liu, M. Li, H. Luo, Q. Liu, and A. L. Swindlehurst, "Integrated sensing and communication with reconfigurable intelligent surfaces: Opportunities, applications, and future directions," *IEEE Wireless Commun.*, vol. 30, no. 1, pp. 50–57, Feb. 2023.
- [18] S. P. Chepuri, N. Shlezinger, F. Liu, G. C. Alexandropoulos, S. Buzzi, and Y. C. Eldar, "Integrated sensing and communications with reconfigurable intelligent surfaces: From signal modeling to processing," *IEEE Signal Process. Mag.*, vol. 40, no. 6, pp. 41–62, Sep. 2023.
- [19] X. Song, J. Xu, F. Liu, T. X. Han, and Y. C. Eldar, "Intelligent reflecting surface enabled sensing: Cramér-rao bound optimization," *IEEE Trans. Signal Process.*, vol. 71, pp. 2011–2026, May 2023.
- [20] Z. Xing, R. Wang, and X. Yuan, "Joint active and passive beamforming design for reconfigurable intelligent surface enabled integrated sensing and communication," *IEEE Trans. Commun.*, vol. 71, no. 4, pp. 2457 – 2474, Feb. 2023.
- [21] R. P. Sankar, S. P. Chepuri, and Y. C. Eldar, "Beamforming in integrated sensing and communication systems with reconfigurable intelligent surfaces," *IEEE Trans. Wireless Commun.*, vol. 23, no. 5, pp. 4017–4031, Sep. 2023.
- [22] Z. Zhang, L. Dai, X. Chen, C. Liu, F. Yang, R. Schober, and H. V. Poor, "Active RIS vs. passive RIS: Which will prevail in 6G?" *IEEE Trans. Commun.*, vol. 71, no. 3, pp. 1707–1725, Dec. 2022.
- [23] Z. Yu, H. Ren, C. Pan, G. Zhou, B. Wang, M. Dong, and J. Wang, "Active RIS aided ISAC systems: Beamforming design and performance analysis," *IEEE Trans. Commun.*, vol. 72, no. 3, pp. 1578 – 1595, Nov. 2023.
- [24] Q. Zhu, M. Li, R. Liu, and Q. Liu, "Joint transceiver beamforming and reflecting design for active RIS-aided ISAC systems," *IEEE Trans. Veh. Technol.*, vol. 72, no. 7, pp. 9636–9640, Feb. 2023.
- [25] Z. Wang, X. Mu, and Y. Liu, "STARS enabled integrated sensing and communications," *IEEE Trans. Wireless Commun.*, vol. 22, no. 10, pp. 6750 – 6765, Feb. 2023.
- [26] Z. Zhang, Y. Liu, Z. Wang, and J. Chen, "STARS-ISAC: How many sensors do we need?" *IEEE Trans. Wireless Commun.*, vol. 23, no. 2, pp. 1085 – 1099, June 2023.
- [27] Z. Zhang, W. Chen, Q. Wu, Z. Li, X. Zhu, and J. Yuan, "Intelligent omni surfaces assisted integrated multi-target sensing and multi-user MIMO communications," *IEEE Trans. Commun.*, Mar. 2024 (Early Access).
- [28] M. Grant and S. Boyd, "CVX: Matlab software for disciplined convex programming, version 2.1," <https://cvxr.com/cvx>, Mar. 2014.
- [29] S. W. Ellingson, "Path loss in reconfigurable intelligent surface-enabled channels," in *IEEE 32nd Annual International Symposium on Personal, Indoor and Mobile Radio Communications (PIMRC)*. IEEE, Oct. 2021, pp. 829–835.
- [30] E. Basar and H. V. Poor, "Present and future of reconfigurable intelligent surface-empowered communications [perspectives]," *IEEE Signal Process. Mag.*, vol. 38, no. 6, pp. 146–152, Oct. 2021.
- [31] K. Zhi, C. Pan, H. Ren, K. K. Chai, and M. ElKashlan, "Active RIS versus passive RIS: Which is superior with the same power budget?" *IEEE Commun. Lett.*, vol. 26, no. 5, pp. 1150–1154, Mar. 2022.
- [32] Z. Yigit, E. Basar, M. Wen, and I. Altunbas, "Hybrid reflection modulation," *IEEE Trans. Wireless Commun.*, vol. 22, no. 6, pp. 4106–4116, Nov. 2022.
- [33] R. Long, Y.-C. Liang, Y. Pei, and E. G. Larsson, "Active reconfigurable intelligent surface-aided wireless communications," *IEEE Trans. Wireless Commun.*, vol. 20, no. 8, pp. 4962–4975, Mar. 2021.
- [34] K. K. Kishor and S. V. Hum, "An amplifying reconfigurable reflectarray antenna," *IEEE Trans. Antennas Propag.*, vol. 60, no. 1, pp. 197–205, Sep. 2011.
- [35] X. Mu, Y. Liu, L. Guo, J. Lin, and R. Schober, "Simultaneously transmitting and reflecting (STAR) RIS aided wireless communications," *IEEE Trans. Wireless Commun.*, vol. 21, no. 5, pp. 3083–3098, Oct. 2021.
- [36] J. Xu, J. Zuo, J. T. Zhou, and Y. Liu, "Active simultaneously transmitting and reflecting (STAR)-RISs: Modelling and analysis," *IEEE Commun. Lett.*, vol. 27, no. 9, pp. 2466 – 2470, June 2023.
- [37] J. Xu, X. Mu, J. T. Zhou, and Y. Liu, "Simultaneously transmitting and reflecting (STAR)-RISs: Are they applicable to dual-sided incidence?" *IEEE Wireless Commun. Lett.*, vol. 12, no. 1, pp. 129–133, Nov. 2022.
- [38] L. G. De Oliveira, B. Nuss, M. B. Alabd, A. Diewald, M. Pauli, and T. Zwick, "Joint radar-communication systems: Modulation schemes and system design," *IEEE Trans. Microw. Theory Techn.*, vol. 70, no. 3, pp. 1521–1551, Nov. 2021.
- [39] X. Shao, C. You, W. Ma, X. Chen, and R. Zhang, "Target sensing with intelligent reflecting surface: Architecture and performance," *IEEE J. Sel. Areas Commun.*, vol. 40, no. 7, pp. 2070–2084, Mar. 2022.
- [40] X. Meng, F. Liu, S. Lu, S. P. Chepuri, and C. Masouros, "RIS-assisted integrated sensing and communications: A subspace rotation approach," in *2023 IEEE Radar Conference (RadarConf23)*. IEEE, May 2023, pp. 1–6.
- [41] X.-D. Zhang, *Matrix analysis and applications*. Cambridge University Press, 2017.
- [42] I. Bekkerman and J. Tabrikian, "Target detection and localization using MIMO radars and sonars," *IEEE Trans. Signal Process.*, vol. 54, no. 10, pp. 3873–3883, Sep. 2006.